**Highlight #1: Structures of Rhodopsin Kinase in Different Ligand States Reveal Key Elements Involved in G Protein-coupled Receptor Kinase Activation**

Rhodopsin (Rho) is the G protein-coupled receptor (GPCR) responsible for visual signal transduction in rod cells. Phosphorylation of light-activated Rho (Rho*) by rhodopsin kinase, also known asGPCRkinase 1 (GRK1), initiates a series of events that rapidly quenches signaling by the receptor. This rapid desensitization is essential for scotopic vision and, in concert with the regeneration of visual pigment, protects rod cells from photodegeneration and permits rapid adaptation to changes in illumination. Phosphorylation of Rho* at multiple sites by GRK1 is also believed to contribute to the reproducibility of the single photon visual response.

Liquid chromatography-tandem mass spectrometry analysis of digested GRK1 proteins was performed using a linear ion trap mass spectrometer (model LTQ) from Thermo-Finnigan coupled with an Ettan MDLC system (GE Healthcare). The obtained data were submitted to Bioworks (Thermo Scientific) by searching the phosphorylation on Ser, Thr, and Tyr. Phosphorylation sites were confirmed by tandem MS2 and/or MS3.

Here we report six crystal structures of rhodopsin kinase (GRK1), revealing not only three distinct nucleotide-binding states of a GRK but also two key structural elements believed to be involved in the recognition of activated GPCRs. The first is the C-terminal extension of the kinase domain, which was observed in all nucleotide-bound GRK1 structures. The second is residues 5–30 of the N terminus, observed in one of the GRK1_(Mg2_)2_ATP structures. The N-terminus was also clearly phosphorylated, leading to the identification of two novel phosphorylation sites by mass spectral analysis. Co-localization of the N-terminus and the C-terminal extension near the hinge of the kinase domain suggests that activated GPCRs stimulate kinase activity by binding to this region to facilitate full closure of the kinase domain.

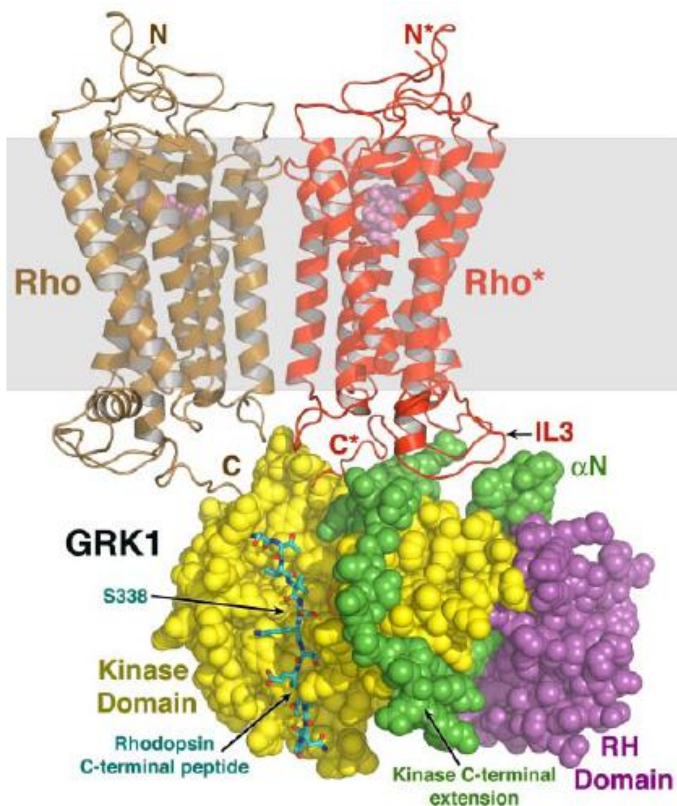


**Figure 1. Conceptual model of GRK1 docked to Rho*.** The closed composite model of GRK1 was docked with a model of an array of Rho molecules (Protein Data Bank code 1N3M) (50), of which two molecules are shown here for clarity. GRK1 is rendered as *spheres*, and the expected lipid bilayer plane is shown as a *transparent gray box*. A monomer of Rho* (*red*) was modeled such that its third cytoplasmic loop (IL3) lies close to the proposed receptor-docking site. Using the PKB-GSK3_ structure (1O6L) as a guide, the C-terminal peptide of Rho* (carbons are colored *cyan*, oxygens are *red*, and nitrogens are *blue*) was modeled docked to the large lobe. The GRK1 active site would have easy access to the C-tail of Rho* or of a neighboring unactivated Rho (*brown*) in the samemembraneplane, allowing high gain phosphorylation of ROS.

**Results from:** Singh, P., Wang, B., Maeda, T., Palczewski, K., Tesmer, J.J.D. Structures of rhodopsin kinase in different ligand states reveal key elements involved in G protein-coupled receptor kinase activation, *J Biol Chem,* 283: 14053-14062, 2008.

**Highlight #2: Proteomics Analysis Identifies Molecular Targets Related to Diabetes Mellitus Associated Bladder Dysfunction**

Diabetic bladder dysfunction is among the most common complications associated with diabetes mellitus. The disease is not life threatening; however, it is associated with several debilitating urological symptoms. It appears that up to 80% of patients with diabetes may eventually develop some type of bladder dysfunction. Unfortunately, there are few systems biology studies focusing on the initiation, development, and progression of the bladder dysfunction in diabetic patients or relevant animal models.

In exploring the possible causes of bladder dysfunction at the proteome level during the initiation, and progression of the disease, protein expression profiles in rat bladder smooth muscles were compared between animal models of STZ-induced diabetes mellitus (STZ-DM) and age matched controls (AMC) at one week and two months after induction of hyperglycemia with STZ treatment. At each time point, protein samples from four STZ-DM and four AMC rat bladder tissues were prepared independently and analyzed together across multiple DIGE gels using a pooled internal standard sample to quantify expression changes with statistical confidence. A total of 100 spots were determined to be significantly changing among the four experimental groups. A subsequent mass spectrometry analysis of the 100 spots identified a total of 56 unique proteins.

A network analysis of these proteins using Metacore™ suggested induction of transcriptional factors that are too low to be detected by 2D-DIGE and identified an enriched cluster of down regulated proteins that are involved in cell adhesion, cell shape control and motility; including vinculin, intermediate filaments, Ppp2r1a, and extra cellular matrix (ECM) proteins. The proteins that are up-regulated include proteins involved in muscle contraction (eg., Mrlcb, and Ly-GDI), in glycolysis (eg., $\alpha$-enolase, and Taldo1), in mRNA processing (eg., hnRNP A2/B1), in inflammatory response (eg., S-100A9, Anexin1, and ApoA-I), and in chromosome segregation and migration (eg., Tuba1, and Vil2).

Our results suggest that the development of diabetes related bladder complication in this model involves the down regulation of structural and ECM proteins in smooth muscle that are essential for the normal muscle contraction and relaxation but also induces proteins that are associated with cell proliferation and inflammation that may account for some of the functional deficits known to occur in diabetic complications of bladder.

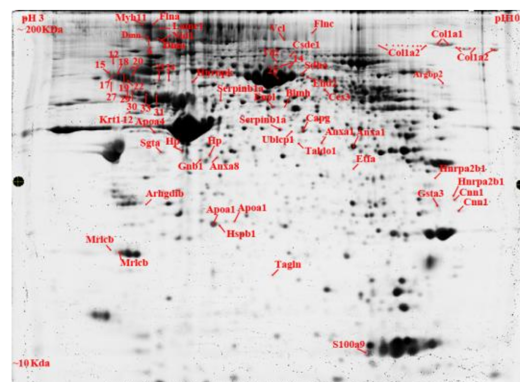


Figure 1

Figure 2

**Figure 1**. **The 2D map of deep purple labeled bladder smooth muscle proteins indicating pick location of subset of proteins that changed in response to STZ-induced diabetes**. Orientation of the pH gradients is indicated on the horizontal axes from 3 pH unit (left) to 10 pH unit (right), and approximate apparent molecular mass ranges are indicated along the vertical axes 10 kDa (bottom) to 200 kDa (top).

**Figure 2. Protein networks associated with the proteins differentially expressed in response to STZ-induced diabetes. Individual proteins are represented as nodes, and the different shapes of the nodes represent the functional class of the proteins. The edges define the relationships of the nodes: the arrowheads indicate the direction of the interaction.**

**Results from:** Yohannes, E., Chang, J., Christ, G.J., Davies, K.P., Chance, M.R. Proteomics Analysis Identifies Molecular Targets Related to Diabetes Mellitus Associated Bladder Dysfunction. *Mol. Cell Prot.,* 7: 1270-1285, 2008.

**Highlight #3: Functional Consequences of Conformational Changes in the ClpA Hexamer and the ClpP N-terminus**

ATP-dependent proteases are responsible for a variety of essential cellular regulatory functions, the most notable of which are the dissolution of protein aggregates and the degradation of unwanted proteins. Understanding the conformational changes that enable these proteases to manipulate their substrates is a useful first step in designing agents to modulate bacterial physiology by activating or inhibiting these molecular machines. In a collaborative effort, the Case Western Reserve University Chance group and the Massachusetts Institute of technology Licht group used x-ray synchrotron footprinting and kinetic studies to investigate these conformational changes in the ClpAP protease complex.

Existing hexameric models of the ClpA chaperone based on the ADP-bound monomeric crystal structure provided a basis for comparison for the footprinting data. The data differed substantially from the models in two parts of the structure: the D1 sensor 1 domain and the D2 loop region. The results suggest that these two regions can access alternate conformations in which they are significantly less solvent accessible. In combination with previously reported structural data, the footprinting data provide support for a revised model in which the D2 loop contacts the D1 sensor 1 domain in the ATP-bound form of the complex (figure 1). These data provide the first direct experimental support for the nucleotide-dependent D2 loop conformational change previously proposed to mediate substrate translocation.

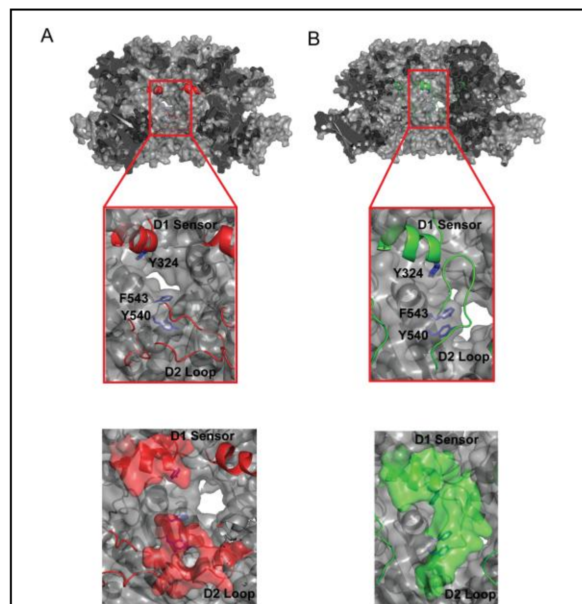


**Figure 1.** Cross-Section of the ClpA hexamer illustrating the pore region (A) a previous hexameric model (Hinnerwisch et al., 2005). (B) footprinting model. The sequences containing the D1 sensor 1 region (318–333) and the D2 loop (526–538) peptides are highlighted and labeled. Bottom figures depict the D1 Sensor 1 and D2 Loop regions in space-fill form.

Footprinting and kinetic studies were used to characterize functionally important conformational changes of the ClpP N-termini. The data suggest a model for proteolysis (figure 2) by wild-type ClpAP in which an interaction with the ATP-bound form of ClpA causes the ClpP N-termini to assume the “up” conformation. This conformational change opens the ClpP axial pore, providing substrate access to the active sites and enabling formation of the acyl-enzyme intermediate. Re-entry of the ClpP N-termini into the axial pore leads to hydrolysis of the acyl-enzyme intermediate and escape of the product via the equatorial pores. An important unresolved question is exactly how ATP-driven conformational changes of ClpA are coupled to the conformational changes of ClpP that regulate acyl-enzyme reactivity. It may be that motions of the ClpA D2 loop, proposed to drive substrate translocation, also drive ClpP conformational changes. Further footprinting and kinetic studies are expected to help resolve this question.

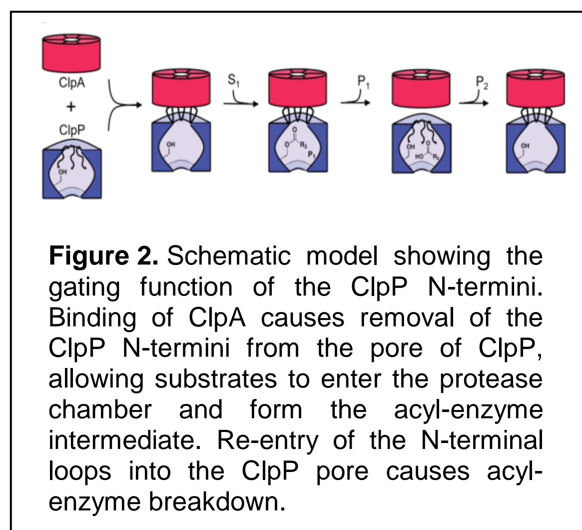


**Figure 2.** Schematic model showing the gating function of the ClpP N-termini. Binding of ClpA causes removal of the ClpP N-termini from the pore of ClpP, allowing substrates to enter the protease chamber and form the acyl-enzyme intermediate. Re-entry of the N-terminal loops into the ClpP pore causes acyl-enzyme breakdown.

**Results from:**

Bohon J., Jennings, L.D., Phillips, C.M., Licht, S., Chance, M.R. (2008) Synchrotron Protein Footprinting Supports Substrate Translocation by ClpA via ATP-Induced Movements of the D2 Loop. *Structure* **16**, 1157-1165.

Jennings, L.D., Bohon, J., Chance, M.R., Licht, S. (2008) The ClpP N-terminus Coordinates Substrate Access with Protease Active Site Reactivity. *Biochemistry*, in press.

**Highlight #4: Effect of methylglyoxal modification on stress-induced aggregation of client proteins and their chaperoning by human *α*A-crystallin**

*α*A-Crystallin prevents protein aggregation under various stress conditions through its chaperone-like properties. Previously, we demonstrated that MGO (methylglyoxal) modification of *α*A-crystallin enhances its chaperone function and thus may affect transparency of the lens. During aging of the lens, not only *α*A-crystallin, but its client proteins are also likely to be modified by MGO. We have investigated the role of MGO modification of four model client proteins (insulin, *α*-lactalbumin, alcohol dehydrogenase and *γ*-crystallin) in their aggregation and structure and the ability of human *α*A-crystallin to chaperone them. We found that MGO modification (10–1000 *μ*M) decreased the chemical aggregation of insulin and *α*-lactalbumin and thermal aggregation of alcohol dehydrogenase and *γ*-crystallin. Surface hydrophobicity in MGO-modified proteins decreased slightly relative to unmodified proteins. HPLC and MS analyses revealed argpyrimidine and hydroimidazolone in MGO-modified client proteins. The degree of chaperoning by *α*A-crystallin toward MGO-modified and unmodified client proteins was similar. Co-modification of client proteins and *α*A-crystallin by MGO completely inhibited stress-induced aggregation of client proteins. Our results indicate that minor modifications of client proteins and *α*A-crystallin by MGO might prevent protein aggregation and thus help maintain transparency of the aging lens.

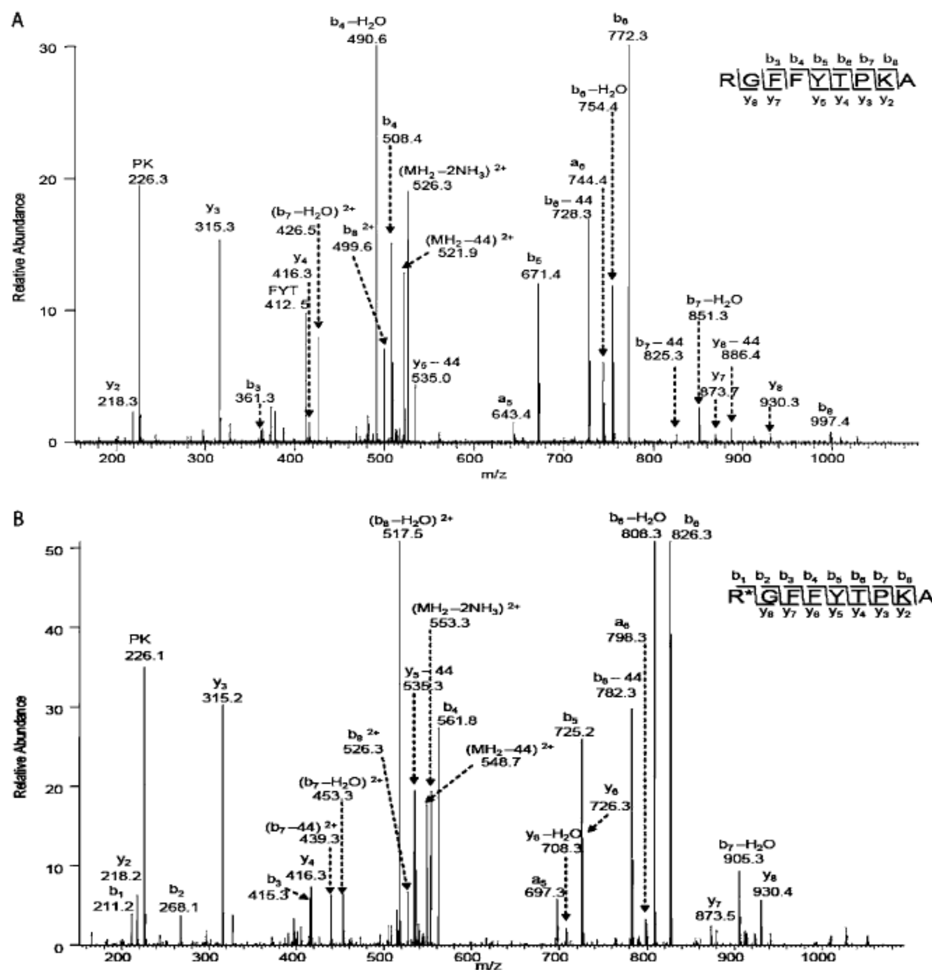


**Figure 1. MS/MS spectra of peptides derived from MGO-treated and untreated insulin.** MS/MS spectra of (**A**) the peptide R22GFFYTPKA30 (with an m/z of 543.5) from untreated insulin and (**B**) R22*GFFYTPKA30 (with an m/z of 570.9) from MGO-modified insulin. Both precursor ions are doubly charged.

**Results from:** Biswas, A., Wang, B., Miyagi, M., Nagaraj, R.H. Effect of methylglyoxal modification on stress-induced aggregation of client proteins and their chaperoning by human alphaA-crystallin, *Biochem J*, *409,* 771-777, 2008.

## Highlight #5: Concurrent Nucleation of 16S Folding and Induced Fit in 30S Ribosome Assembly

Rapidly growing cells produce thousands of new ribosomes each minute, in a tightly regulated process that is essential to cell growth. How the Escherichia coli 16S ribosomal RNA and the 20 proteins that make up the 30S ribosomal subunit can assemble correctly in a few minutes remains a challenging problem, partly because of the lack of real-time data on the earliest stages of assembly.

The Woodson group from Johns Hopkins University collected radiolytic footprinting data from the X28C beamline of Case Western Reserve University. Time-resolved hydroxyl radical footprinting was used to map changes in the structure of the rRNA within 20 milliseconds after the addition of total 30S proteins. Helical junctions in each domain fold within 100ms. In contrast, interactions surrounding the decoding site and between the 59, the central and the 39 domains require 2–200 seconds to form.

Previous studies indicated that ribosome assembly is not completely cooperative, demonstrating the need for several nucleation sites. The lack of complete cooperativity, and the differences between the time-dependence of 16S folding and the assembly map revealed by kinetic footprinting of the nucleotide bases, support the conclusion that assembly proceeds in parallel through intermediates with different subsets of proteins. Radiolytic footprinting allows snapshots of individual RNA and protein interactions to be taken as they emerge in real time. Therefore, the Woodson group was able to show that 30S assembly nucleates concurrently from different points along the rRNA.

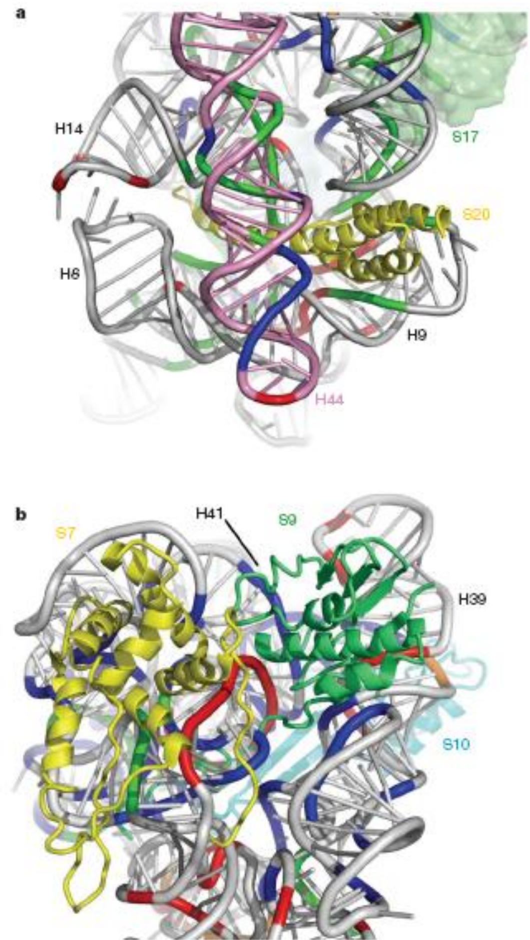


**Figure 1.** Stepwise assembly of RNA and protein interactions. **a.** Protein S20 (yellow ribbon) contacts the 30S body in the 59 domain (grey) earlier than helix H44 in the 39 minor domain (pink). **b.** Proteins S7 (yellow) and S9 (green) protect a segment of their binding site immediately (red), whereas nucleotides at the interface between the subdomains are protected slowly (blue).

**Results from:** Adilakshmi, T., Bellur, D.L., Woodson, S.A. Concurrent nucleation of 16S folding and induced fit in 30S ribosome assembly, *Nature*, 2008, in press.

**Highlight #6: The structural basis of serpin polymerization studied by hydrogen/deuterium exchange and mass spectrometry**

The serpinopathies are a group of inherited disorders that share as their molecular basis the misfolding and polymerization of serpins – an important class of protease inhibitors. Depending on the identity of the serpin, conditions arising from polymerization include emphysema, thrombosis, and dementia. The structure of serpin polymers is thus of considerable medical interest. Wild type α1-antitrypsin will form polymers upon incubation at moderate temperatures and has been widely used as a model system for studying serpin polymerization. Using hydrogen/deuterium exchange and mass spectrometry, we have obtained molecular level structural information on the α1-antitrypsin polymer. We find that the flexible reactive center loop becomes strongly protected upon polymerization. We also find significant increases in protection in the center of β-sheet A and in helix F. These results support a model in which linkage between serpins is achieved through the insertion of the reactive center loop of one serpin into β-sheet A of another. We have also examined the heat induced conformational changes preceding polymerization. We find that polymerization is preceded by significant destabilization of β-sheet C. Based on our results, we propose a mechanism for polymerization in which β-strand 1C is displaced from the rest of β-sheet C through a binary serpin-serpin interaction. Displacement of strand 1C triggers further conformational changes, including the opening of β-sheet A, and allows for subsequent polymerization.

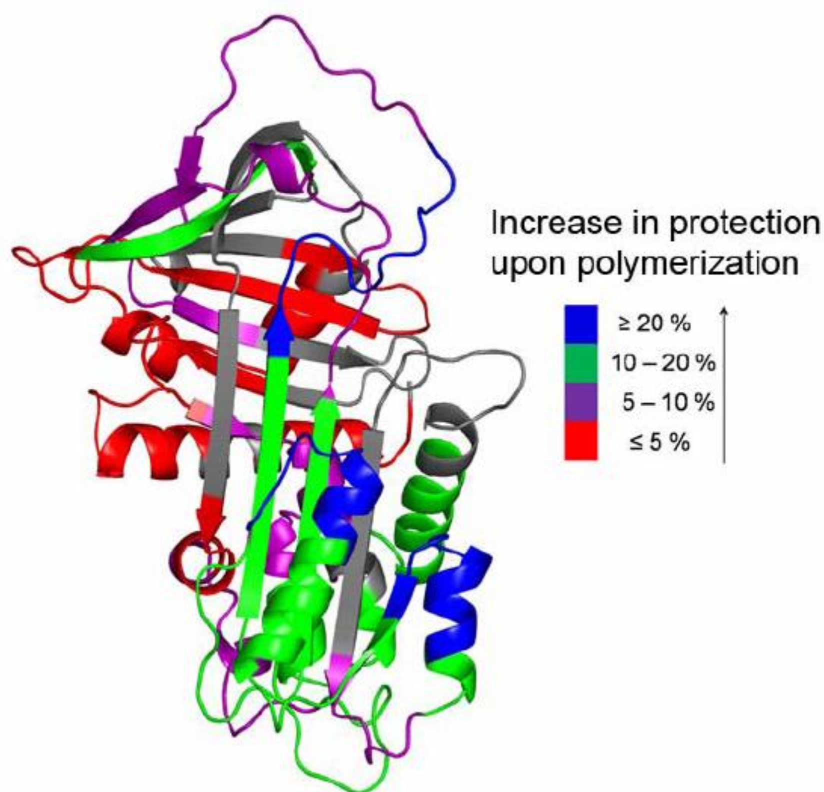


**Figure 1.** Differences in hydrogen exchange (at 5000 seconds) between monomeric and polymeric α1-AT mapped on to the 3 dimensional structure (1qlp). Darker colors represent larger decreases in observed exchange (i.e., increased protection) in the polymer as compared to the monomer.

**Results from:** Tsutsui, Y., Kuri, B., Sengupta, T., Wintrode, P.L. The structural basis of serpin polymerization studied by hydrogen/deuterium exchange and mass spectrometry, *J. Biol. Chem.*, in press.